ROTATING MACHINERY TECHNOLOGY, INC.

PRECISION BEARINGS AND SEALS
TURBOMACHINERY REPAIR
ROTORDYNAMIC ANALYSES

STABILIZING TURBOMACHINERY WITH PRESSURE DAM BEARINGS

John C. Nicholas

December 1994

published in

ENCYCLOPEDIA OF FLUID MECHANICS
VOLUME 2, DYNAMICS OF SINGLE-FLUID FLOWS AND MIXING
GULF PUBLISHING COMPANY

STABILIZING TURBOMACHINERY WITH PRESSURE DAM BEARINGS

John C. Nicholas, Ph.D.
Chief Engineer
Rotating Machinery Technology, Inc.
Wellsville, New York 14895

INTRODUCTION

Although tilting pad bearings are currently used in the design of a large percentage of the world's high speed, multistage turbomachinery, there still exists a large class of rotors that are designed or are presently operating with fixed-lobe bearings. Examples include axial compressors, steam turbines, hot gas expanders, and many older model centrifugal compressors. One characteristic of machines that operate successfully with fixed-bore bearings is a low speed-to-weight ratio. This indicates a relatively stiff shaft design and consequently a fundamental mode shape that is nearly rigid. A rigid body mode ensures a significant response at the bearing locations to allow the bearing damping to be effective in suppressing shaft vibrations [1].

A major problem with many plain and axial-groove bearings is that they exhibit a relatively low oil whirl instability threshold speed that produces a reexcitation of the rotor's first fundamental natural frequency [2, 3]. Oil whirl is a high speed and/or light load condition. For example, a plain cylindrical journal bearing with a 6.0 mil radial clearance could not operate above 6,000 rpm without whirling. However, many other fixed-bore bearing designs are effective in suppressing oil whirl and thus can operate above 6,000 rpm without becoming unstable. The most commonly used of these are the pressure dam or step journal bearing [4–11] and the multi-lobe bearing [11–14].

The stability characteristics of plain cylindrical bearings are primarily controlled by the bearing clearance; the tighter the clearance, the higher the instability threshold speed. However, tight clearance bearings present other problems that make them undesirable. For example, oil flow is lower, power loss is higher, and thermal growth of the journal may cause the bearing to wipe. Many

bearing-induced instability problems in the field are caused by bearing clearances that have increased due to wear from oil contamination, poor filtration, and/or repeated starts and slow rolling with boundary lubrication.

Thus, it is desirable to analyze and design an effective fixed-bore anti-whirl bearing that is easily manufactured, relatively insensitive to design tolerances, and available for quick retrofits in existing plain bearing inserts. The pressure dam bearing falls into this category. The details of the surface inside the pocket are of secondary importance since the side lands hold the flow and the pressure. The hydrodynamic load created by the pocket provides the increased margin of stability for step bearings compared to plain bearings [6–8]. Finally, the tolerance on the pocket depth is not as critical as lobe-clearance tolerances for multilobe bearings. Tolerances on the lobe radius for multilobe bearings are often on the order of ± 1.0 mils. These tolerances can be relaxed for pocket bearing profiles, which therefore reduces manufacturing costs. Typical pocket depth tolerances are often ± 2.5 mils.

Pressure dam or step journal bearings have long been used to improve the stability of turbomachinery as replacements for plain journal or axial groove bearings. In many cases, these bearings provide a quick and inexpensive fix for machines operating at high speeds near or above the stability threshold. For example, a plain cylindrical axial-groove bearing can easily be removed from a machine displaying subsynchronous vibration. Milling a step in the top pad of the proper size and location may be all that is necessary to eliminate the stability problem. This is much less expensive and faster than installing tilting pad bearings that may require a change in the bearing housing.

A large percentage of the rotors used in the rotating equipment industry operate on vendor installed or retrofitted pressure dam bearings. The most common applications are steam turbines and gear boxes. In high speed gear boxes, the gear loading may vary from several thousand to only a few hundred pounds. This large variance in load is often accompanied by a change in load direction. An example is the gear box between a motor/generator and a start-up steam turbine in a catalytic cracking axial-compressor train. In this particular application, step bearings are used to ensure stable operation when the gear loading is small.

The purpose of this paper is to describe how the pressure dam bearing suppresses oil whirl and to identify the important design parameters necessary to optimize its stability performance. These concepts are extremely important for both rotating equipment vendors and users who design step journal bearings either as original equipment or as retrofits replacing plain bearings.

INERTIA AND TURBULENCE EFFECTS

The majority of oil-lubricated journal bearings operate in the slow viscous flow regime where the viscous forces are much greater than the inertia forces. This is certainly true for a vast majority of the bearings in industrial application where the bearing Reynolds number is usually below 1,500. The Reynolds number is the ratio of inertia forces to viscous forces and, for a journal bearing, is defined as

$$R_e = \frac{\pi R N \rho c}{30\mu} \tag{1}$$

where R = journal radius, in.
N = shaft rotational speed, rpm
ρ = lubricant density, lb-s^2/in.^{4}
c = bearing radial clearance, in.
μ = lubricant viscosity, lb-s/in.^{2}

The analytical solution technique used to solve for the hydrodynamic pressures in a journal bearing neglects inertia forces. Also, turbulence is usually neglected and the flow is assumed laminar. Laminar flow is also a low Reynolds number condition. Thus, these assumptions are valid for most oil-lubricated journal bearings. However, for a pressure dam bearing, the Reynolds number inside the pocket is anywhere from 3 to 20 times the bearing Reynolds number due to the increased pocket

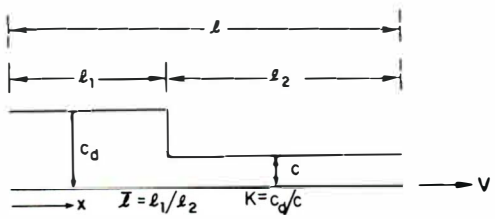

Figure 1. Stepped slider bearing.

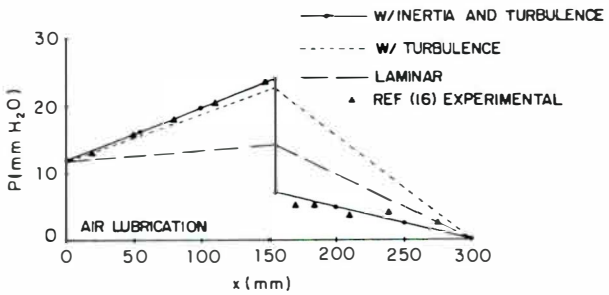

Figure 2. Stepped slider pressure profiles for air lubrication.

clearance. In this region, the flow is turbulent and inertia effects may become significant compared to viscous forces.

To investigate the relative importance of inertia and turbulence, it is instructive to consider a flat-stepped slider bearing as shown in Figure 1. The slider surface is assumed to be infinite in length so that velocities normal into and out of the surface can be ignored. This assumption is not valid for most bearings but it is necessary to include inertia effects in the solution whereas a finite length slider with inertia is an extremely difficult problem. However, the general trends and conclusions based on the infinite solution remain valid for finite length journal bearings. Finite elements are used to solve for the hydrodynamic pressures for the stepped slider [5, 15].

Figure 2 illustrates the hydrodynamic pressure profiles for the infinite flat-stepped slider of Figure 1. Curves are shown for three different analytical techniques. Also, experimental results from Reference 16 are indicated. The analytical solution including inertia and turbulence [5] agrees with the experimental results. Inertialess theory with turbulence over-predicts the load capacity (area under pressure curve) while laminar theory under-predicts the load in the pocket area and over-compensates after the step.

Note that the effect of inertia is to slightly raise the pressure inside the pocket compared to the inertialess case including turbulence. However, after the step the fluid inertia causes a large pressure drop. The overall effect of inertia is to decrease the load-carrying capacity of the stepped slider.

From Figure 2, it appears that inertia must be included to match the experimental results. However, air is the lubricant in Figure 2. Figure 3 shows a comparable plot for oil. Now, the pressure drop after the step is only 10% of the maximum pressure and inertialess theory with turbulence provides a good approximation. Laminar theory again severely underestimates the load.

Load capacity error as a function of film thickness ratio and Reynolds number is plotted in Figure 4 for inertialess theory including turbulence. Oil is the lubricant. For Reynolds numbers below 3,000, the error is less than 10% compared to inertia theory. As the Reynolds number increases, the effect of fluid inertia increases and the error in inertialess theory increases. Note that for film thickness ratios greater than 2.5 the error is negative which means that inertialess theory over-predicts load capacity. Also, negative error implies that, as stated earlier, the effect of fluid inertia is to decrease the load capacity of the slider.

Figure 5 is a series of load curves as a function of pocket clearance ratio, K, and step location, $\bar{\ell}$ (Figure 1). For the stepped slider, these parameters are defined as

$$K = c_d/c \tag{2}$$

$$\bar{\ell} = \ell_1/\ell_2 \tag{3}$$

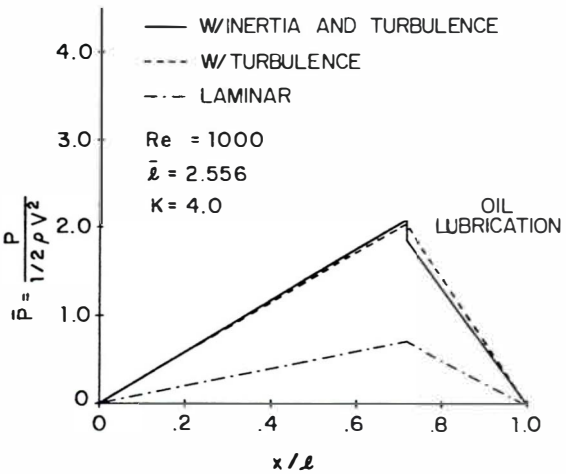

Figure 3. Stepped slider pressure profiles for oil lubrication.

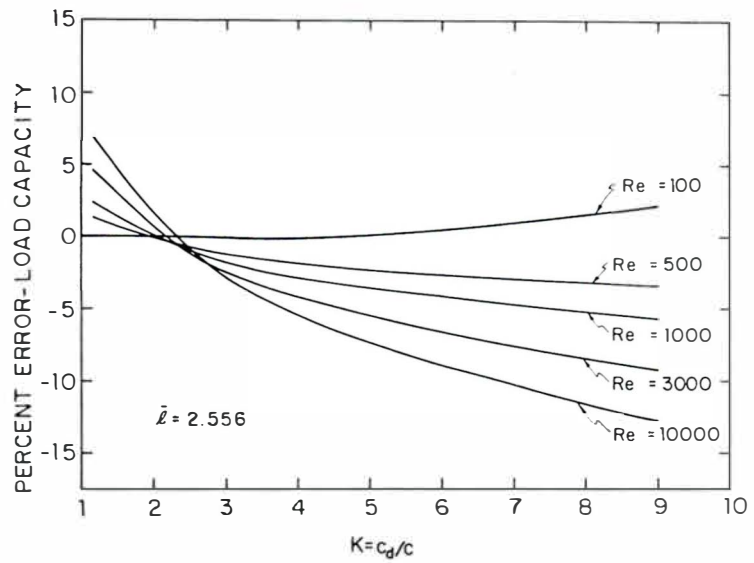

Figure 4. Percent error in load capacity comparing inertia to inertialess theory (both with turbulence effects).

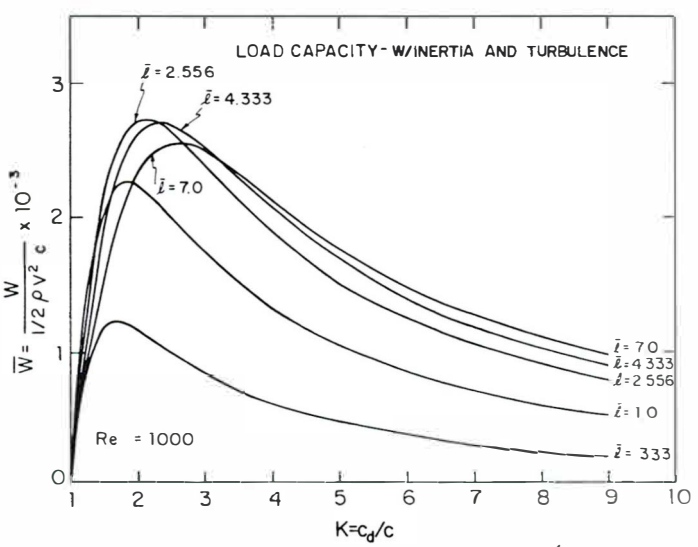

Figure 5. Stepped slider load capacity showing optimum clearance ratio, K, and step location, $\bar{\ell}$.

where c_d = pocket clearance, in.
c = bearing clearance, in.
ℓ_1 = pocket length, in.
$\ell_2 = \ell - \ell_1$, in.
ℓ = total bearing length, in.

Optimum clearance ratios range between 2.0 and 3.0. For K values less than 2.0, the load capacity decreases drastically while for K > 3.0, the load capacity decreases much more gradually. This indicates that the tolerance range on the pocket depth should be above optimum to avoid the steep decrease in load for K values less than 2.0.

The optimum step location from Figure 5 is $\bar{\ell} = 2.556$. As $\bar{\ell}$ increases from the optimum value, only a slight decrease in load capacity is evident. However, as $\bar{\ell}$ decreases from the optimum, a large decrease in load capacity results. For $\bar{\ell} = 2.556$, the pocket length, ℓ_1, is 72% of the total length, ℓ (Figure 1). Thus, pocket designs should be 72% of the total length for near optimum load. Pocket lengths greater than 72% are preferable while lengths less than 72% are not recommended.

It is interesting to note that for laminar flow, the optimum length ratio is $\bar{\ell} = 2.556$. However, the optimum clearance ratio is 1.866 for laminar flow. The clearance ratio optimum increases for turbulent flow since, as the pocket depth increases, the Reynolds number inside the pocket increases and the effect of turbulence on load capacity increases. Thus, there is a trade-off between the pure laminar optimum and the increasing effect of turbulence on load capacity as the pocket depth increases.

SOLUTION TECHNIQUE

From the previous section it was determined that for oil lubrication, inertia effects contribute very little (under 10%) to the hydrodynamic load generated by the step for Reynolds numbers less than 3,000. This is well within the operating range and geometry of the majority of the oil-lubricated journal bearings in industrial application. Thus, neglecting inertia but including the effects of turbulence, the finite pressure dam bearing can be analyzed with some degree of confidence and ease.

Most pressure dam bearings have two oil supply grooves located in the horizontal plane as shown in Figure 6. For a downward- (negative y-direction) directed load corresponding to a portion of the rotor weight, a pocket is cut in the upper half of the bearing with the end of the pocket (the step or dam) located in the second quadrant for counter-clockwise shaft rotation. The pocket has side

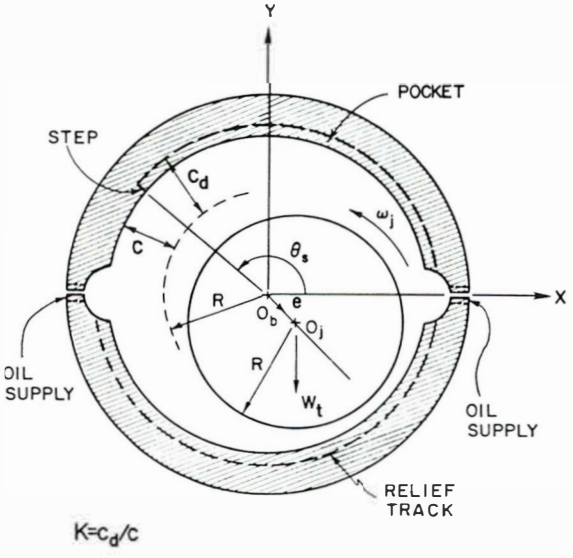

Figure 6. Pressure dam or step journal bearing schematic, side view.

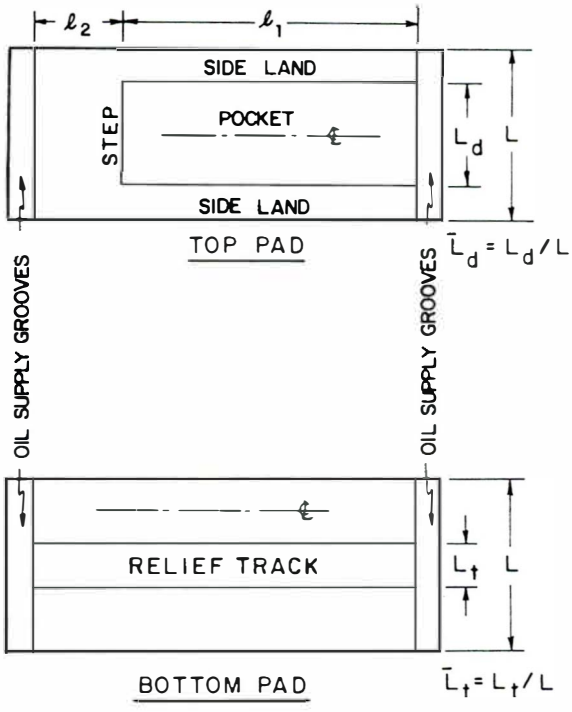

Figure 7. Pressure dam or step journal bearing schematic, top and bottom pads.

lands to hold the pressure and flow as shown in Figure 7. A circumferential relief groove or track is sometimes grooved in the bottom half of the bearing as illustrated in Figures 6 and 7. Both of these effects (dam and relief track) combine to increase the operating eccentricity of the bearing compared to a plain cylindrical bearing.

Investigating the stability characteristics of the pressure dam bearing necessitates the calculation of the bearing's linearized dynamic stiffness and damping coefficients. To this end, a finite element solution technique [15] is again used to solve for the hydrodynamic pressures created by the oil film between the bearing and journal. Each pad of the bearing is divided up into finite elements as indicated in Figure 8 using an automatic mesh generation scheme. The mass rate of flow across the step is conserved without requiring special conditions as with finite differences, an alternate

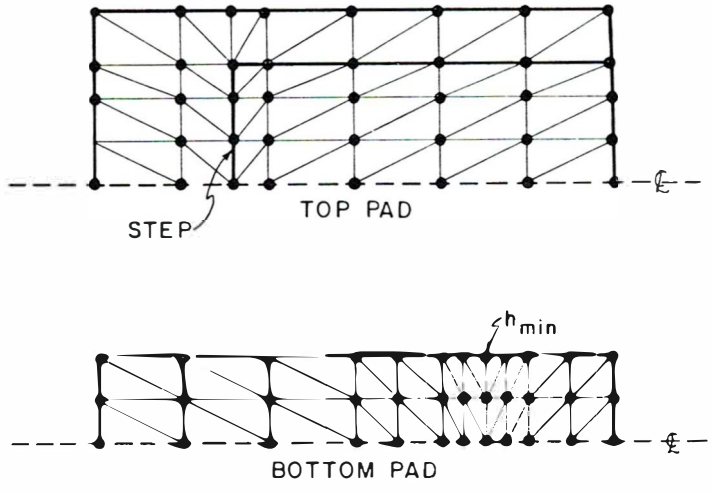

Figure 8. Dividing the pressure dam bearing into finite elements.

solution technique [15]. Nodes in the bottom pad are concentrated around the minimum film thickness where the change in the hydrodynamic pressure is the greatest.

The load capacity of the pressure dam bearing is obtained by integrating the hydrodynamic pressures while linearized dynamic coefficients are determined with small numerical perturbations about the bearing equilibrium position. The equilibrium position is determined by a simple force balance between the resultant hydrodynamic load and the external load. Turbulence effects are included by calculating the local Reynolds number for each element around the bearing and correcting the local viscosity [6].

STABILITY

Prior to in investigating the optimum pressure dam bearing stability configuration, the effect of a stepped pocket on the journal compared to a plain bearing may be easily seen on a bearing eccentricity plot. Figure 9 shows the bearing eccentricity ratio as a function of the Sommerfeld number, a bearing speed parameter. The bearing eccentricity ratio is the amount the journal is offset in the bearing, e (Figure 6) divided by the bearing radial clearance, c. Three curves are plotted on Figure 9. Two different pressure dam bearings with steps located at 125 and 160 degrees are compared to the plain journal bearing curve. All length-to-diameter ratios (L/D) are 1.0.

At high Sommerfeld numbers (light loads and/or high speeds), the journal bearing eccentricity approaches zero and the journal runs centered in the bearing. This condition leads to unstable operation. However, the pressure dam bearing eccentricity either approaches some minimum value or increases as the Sommerfeld number increases.

At high speeds and/or light loads, the step creates a loading that maintains a minimum operating eccentricity. That is, as speed is increased, the bearing eccentricity does not approach zero as it would for plain journal bearings. The eccentricity approaches some minimum value or may even

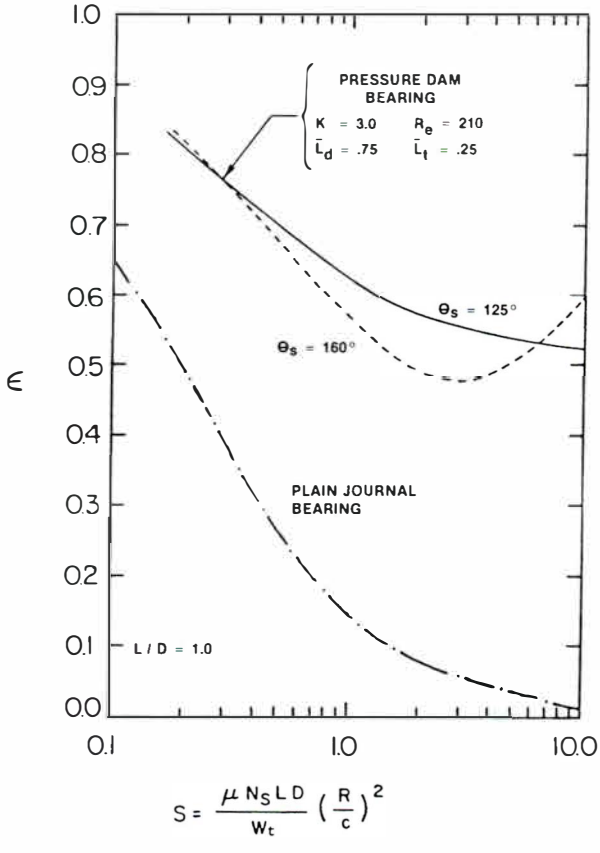

Figure 9. Pressure dam and plain journal bearing eccentricity ratios.

increase with increasing speed due to the step loading. Thus, a properly design step bearing would operate at a moderate eccentricity even at high Sommerfeld numbers. This condition helps to stabilize the pressure dam bearing in the high Sommerfeld number range.

To investigate the stability of a journal in a bearing, the dimensionless stability threshold speed parameter, $\bar{\omega}$ is used [6]. This parameter gives the speed at which the journal becomes unstable in a particular bearing. In this formulation, the shaft is assumed rigid. The effect of a flexible shaft is to lower the instability threshold speed [9]. For horizontal rotors, the threshold speed can be calculated from

$$N_t = 187.6\,\bar{\omega}(c)^{-1/2} \tag{4}$$

where N_t = instability threshold speed, rpm
c = bearing radial clearance, in.
$\bar{\omega}$ = bearing stability parameter, dim

The stability parameter is calculated as a function of the Sommerfeld number from the bearing's stiffness and damping coefficients [9]. Thus, for a given Sommerfeld number corresponding to the bearing's operating conditions, $\bar{\omega}$ may be calculated directly from the dynamic characteristics or determined from a bearing stability plot. The rigid shaft instability threshold speed can then be calculated from Equation 4. For example, for Sommerfeld numbers greater than 0.1, $\bar{\omega} = 2.3$ for a plain journal bearing. For a 6 mil radial clearance and using Equation 4, $N_t = 5{,}570$ rpm. This means that a plain journal bearing operating above $S = .1$ in a horizontal rotor with a 6 mil radial clearance will become unstable above 5,570 rpm.

Of course, bearings cannot be designed based solely on this parameter. However, insight into step journal bearing design may be gained by examining and comparing $\bar{\omega}$ for different step bearing geometries.

Figure 10 compares the stability characteristics of the plain journal, two-axial groove and grooved lower half bearings to two types of pressure dam bearings. The stability threshold speed, $\bar{\omega}$, is plotted against the Sommerfeld number, S. Also indicated at the top is the bearing eccentricity ratio, ϵ for all five bearings. Bearing numbers 1 and 2 are the plain journal and two-axial groove bearings, respectively. Note that at high Sommerfeld numbers the stability curves for each bearing approach asymptotic values of $\bar{\omega} = 2.3$ (plain journal) and $\bar{\omega} = 2.05$ (2 axial groove).

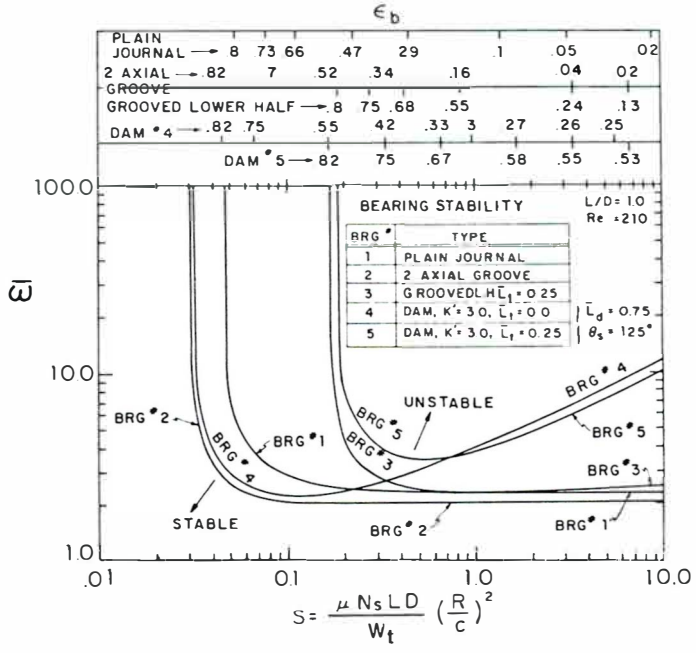

Figure 10. Stability map comparing pressure dam bearing to plain journal, two axial groove and grooved lower half bearings.

Bearing number 3 is the grooved lower half bearing. This bearing is simply a two-axial groove bearing with a circumferential relief track or groove cut in the lower half. In this case, the relief track axial-length ratio (Figures 6 and 7) is $\bar{L}_t = 0.25$ (the relief track is 25% of the bottom pad). A considerable increase in the infinite stability region is evident. That is, the plain journal bearing is theoretically stable at all speeds below a Sommerfeld number of .048 while the grooved lower half bearing increases this range of infinite stability by a factor of 3 to $S \leq 0.17$. The relief track removes part of the bearing load-carrying surface for the bottom pad thereby forcing the bearing to operate at a higher eccentricity ratio. Essentially no increase in stability is seen at high Sommerfeld numbers.

While a bearing designed to operate in the infinite stability region may appear to be advantageous, this design should be avoided since large eccentricities result ($\epsilon \geq 0.8$). A bearing functioning at $\epsilon = 0.8$ at the operating speed may not be able to support the load at idle speed or during slow rolling of the rotor. An exception would be a gear box bearing where the gear load is reduced as speed decreases.

Bearing number 4 is a pressure dam bearing with $K = 3.0$ (pocket clearance three times as large as the bearing clearance) and $\bar{L}_t = 0.0$ (no relief track). For this case, the stability is increased compared to the journal bearing at high Sommerfeld numbers while the region of infinite stability is less. As discussed previously, at high Sommerfeld numbers, the step forces the journal to operate at a moderate eccentricity. From the top of Figure 10, bearing number 4 operates at an eccentricity ratio of $\epsilon = 0.25$ at $S = 5.5$. This moderate eccentricity provides the favorable stability characteristics at high Sommerfeld numbers for this step journal bearing.

The effect of varying the clearance ratio, K, on stability is shown in Figure 11. For a pressure dam bearing, the clearance ratio is defined as (see Figure 6):

$$K = c_d/c$$

where c_d = pocket radial clearance, in.
c = bearing radial clearance, in.

For the infinite-stepped slider, the optimum clearance ratio as far as load capacity is concerned is approximately $K = 3.0$ (Figure 5). Bearing number 3 has a clearance ratio of $K = 3.0$ and provides

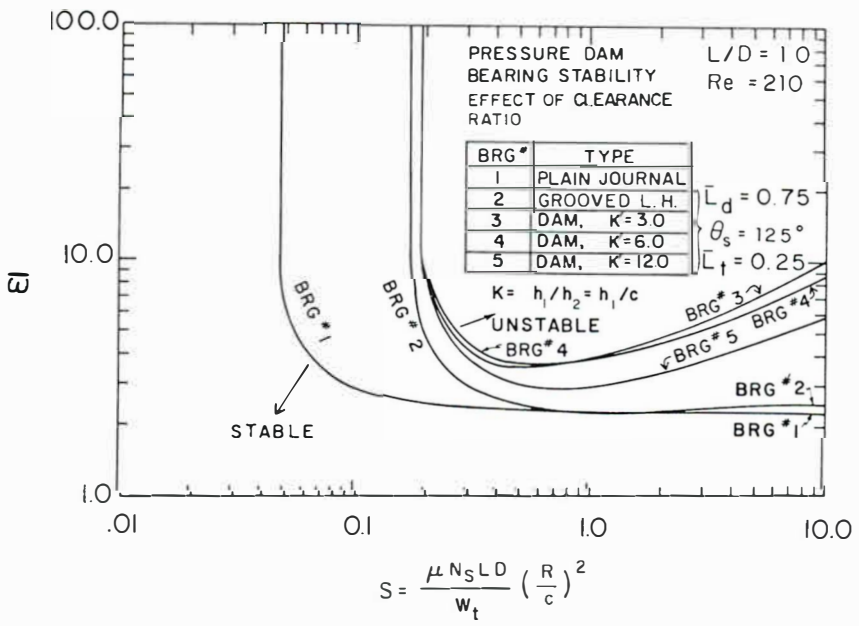

Figure 11. Effect of clearance ratio on pressure dam bearing stability.

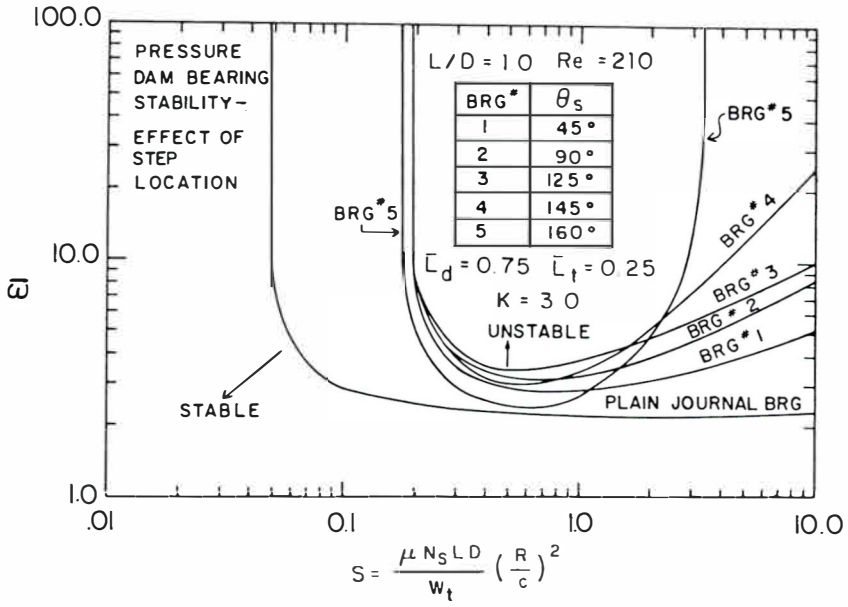

Figure 12. Effect of step location on pressure dam bearing stability.

the best stability characteristics. Bearing number 4 with K = 6.0 is only slightly less superior (a 10% decrease at S = 10.0). A 40% decrease in stability is evident for step bearing number 5 (K = 12.0) when compared to the K = 3.0 bearing at S = 10.0. The stability curves for bearing number 1 (plain journal) and number 2 (grooved lower half) are also included in Figure 11 for comparison.

Figure 12 illustrates the effect of changing the step location on stability. The step is located by the angle, θ_s (Figure 6) measured with rotation, counter-clockwise from the positive horizontal (+X) axis. From the infinite-stepped slider analysis (Figure 5), the optimum step location as far as load capacity is concerned is $\bar{\ell} = 2.556$. This corresponds to approximately $\theta_s = 125°$. This optimum θ_s does provide the optimum stability for $0.2 \leq S \leq 1.7$. However, for $S > 1.7$, bearing number 5 with $\theta_s = 160°$ is more stable. In fact, this bearing has two regions of infinite stability ($S \leq 0.17$ and $S \geq 3.4$). As θ_s decreases from 160°, stability decreases at high Sommerfeld numbers.

In summary, the optimum Sommerfeld number range for designing a pressure dam bearing to increase stability is $S \geq 2.0$. At these high S values, the important design parameters are the clearance ratio, K, and the step location, θ_s. The optimum clearance ratio in this region is around K = 3.0. A slightly larger clearance ratio is recommended to avoid the sudden drop in load capacity for clearance ratios below 3.0. Increasing K from 3.0 to 6.0 reduces stability only slightly in the high Sommerfeld number region (only a 10% decrease in $\bar{\omega}$ at S = 10.0).

The optimum step location for stability is between $\theta_s = 125°$ and 160° depending on the Sommerfeld number. For $S \geq 2.0$, $\theta_s = 160°$ is the optimum while for Sommerfeld numbers in the range of $0.2 \leq S \leq 2.0$, 125° is the optimum. A good compromise is $\theta_s = 140°$.

A step journal bearing designed with these recommended K and θ_s values could increase the stability parameter, $\bar{\omega}$ by a factor of 10 or more over a plain journal bearing at high Sommerfeld numbers. Also, the step journal bearing would operate at a moderate eccentricity ratio (between $\epsilon = 0.25$ and 0.5) even though the loading is light and/or speed high.

EXPERIMENTAL RESULTS

This section presents results of an experimental study with a three-mass flexible rotor mounted symmetrically between two bearing supports. Four different step bearing geometries and a two-axial-groove bearing are considered. The pressure dam designs include optimum and off-optimum clearance ratios and step locations. Instability onset speeds are determined experimentally and compared to the analytical predictions.

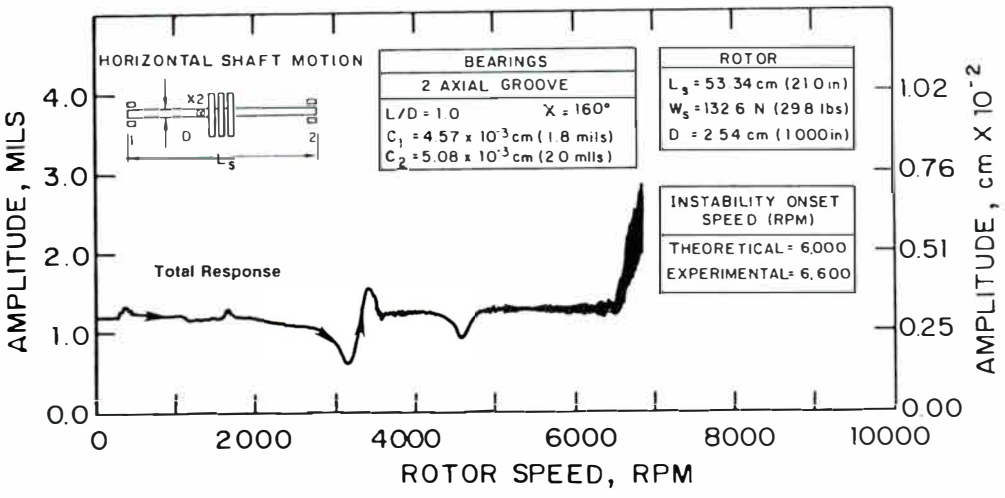

Figure 13. Total response, two axial groove bearings.

The rotor weighs 29.8 lbs, has a bearing span of 21.0 in. and a journal diameter of 1.0 in. A non-contacting probe mounted near the shaft center is used to monitor the horizontal shaft vibration. Additional details of the experimental procedure may be found in References 8, 17, and 18.

Ideally, each bearing was to have a 2.0 mil radial clearance. However, due to difficulties in manufacturing, the radial clearance ranged from 1.8 to 2.5 mils. The clearance was measured cold with a dial micrometer. Several readings were taken and the average value used.

To obtain the experimental instability onset speed, the rotor is accelerated until a large subsynchronous vibration component is observed. Speed-amplitude plots are shown here for the five test cases. In two cases, frequency spectrums are also included.

Figure 13 illustrates the total rotor response with two-axial-groove bearings. Figure 14 is a frequency spectrum for the same case. The subsynchronous component first appears at about N = 6,600 rpm. Note that Figure 14 indicates that the oil whirl instability manifests itself as a reexcitation of the rotor's first fundamental natural frequency of 3,000 cpm.

The theoretically predicted instability onset speed is 6,000 rpm. To obtain this onset speed, the speed-dependent stiffness and damping characteristics are used as input data to a stability computer program that employs a transfer matrix solution. The mass-elastic model of the rotor is also input data to the stability program. A full stability analysis is necessary to accurately predict the threshold speed of a flexible rotor. If Equation 4 is used with c = 1.9 mils and $\bar{\omega} = 2.05$, the resulting threshold

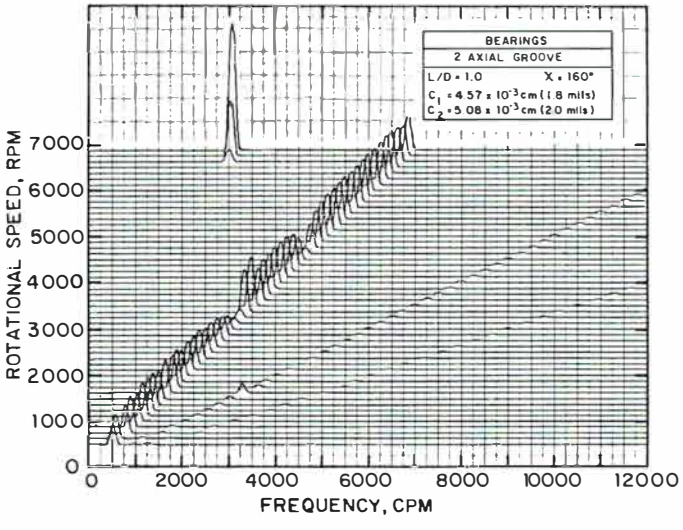

Figure 14. Frequency spectrum, two axial groove bearings.

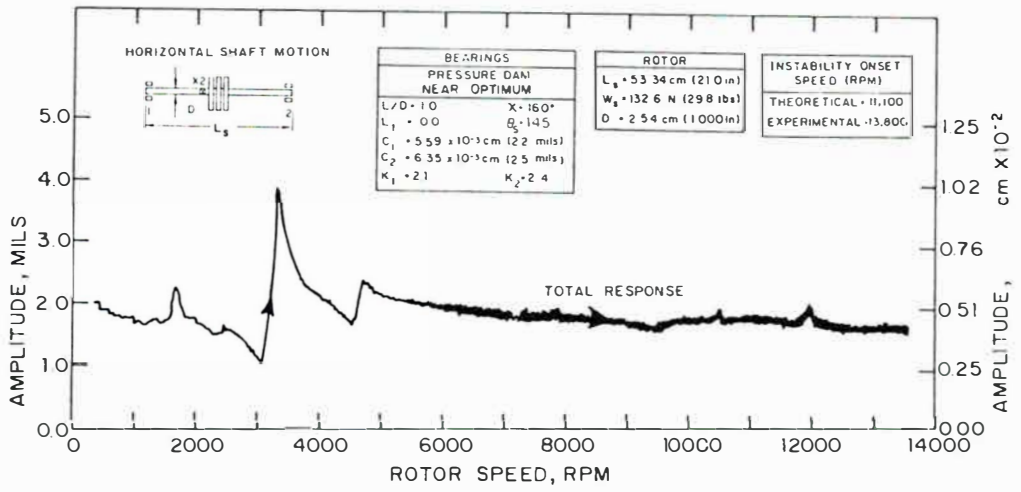

Figure 15. Total response, near optimum pressure dam bearings.

speed is N_t = 8,823 rpm. Thus, the effect of shaft flexibility is to lower the threshold from the rigid rotor prediction of 8,823 rpm down to 6,000 rpm. Caution is necessary when using Equation 4 and the resulting N_t should be viewed as the highest possible instability speed obtainable for the given bearing.

The total response for a near optimum pressure dam bearing design (K = 2.1, and 2.4, and θ_s = 145°) is shown in Figure 15 with a corresponding frequency spectrum in Figure 16. The rotor was run up to maximum speed without a large subsynchronous component appearing. The theoretical prediction is 11,100 rpm.

The effect of increasing the pocket depth from the near optimum case of Figures 15 and 16 is illustrated in Figures 17 and 18. Figure 17 shows the total response with clearance ratios of 6.6 and 8.6. The experimental threshold speed is 8,900 rpm, and the theoretical threshold speed is 8,850 rpm. These speeds are reduced even further for clearance ratios of 11.7 and 8.3 (Figure 18). Both experimental and theoretical threshold speeds are 7,800 rpm for this off-optimum case.

Finally, in Figure 19 near-optimum clearance ratios are used but an off-optimum step location of $\theta_s = 90°$ is considered. For this case the experimental threshold speed is 8,600 rpm while the predicted analytical speed is 8,100 rpm.

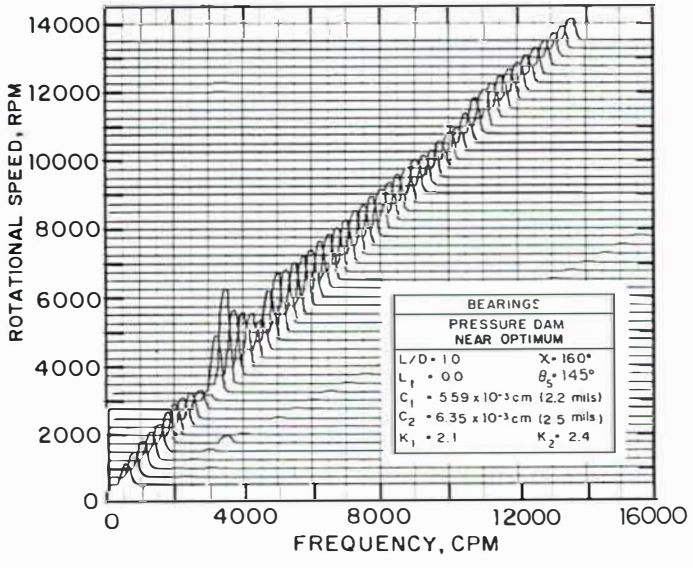

Figure 16. Frequency spectrum, near optimum pressure dam bearings.

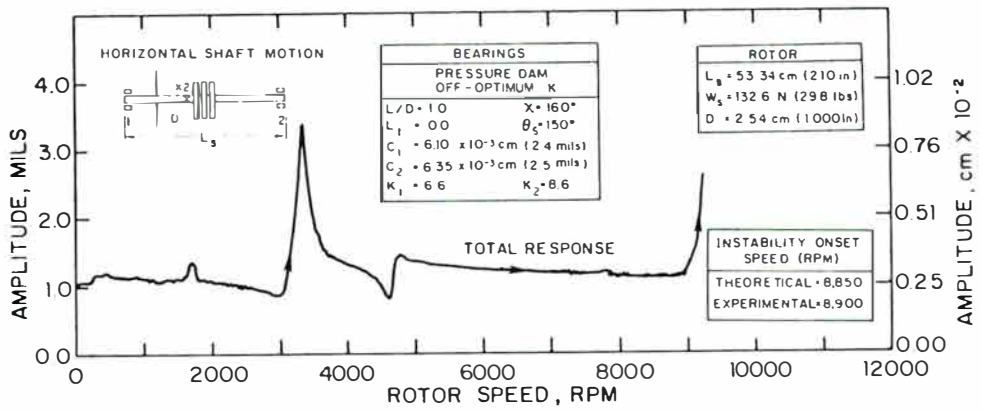

Figure 17. Total response, off-optimum clearance ratio (K = 6.6, 8.6), pressure dam bearings.

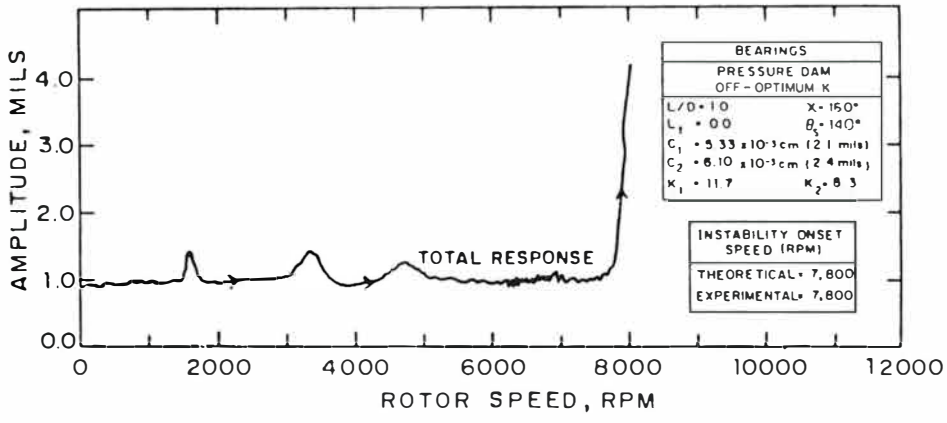

Figure 18. Total response, off-optimum clearance ratio (K = 11.7, 8.3), pressure dam bearings.

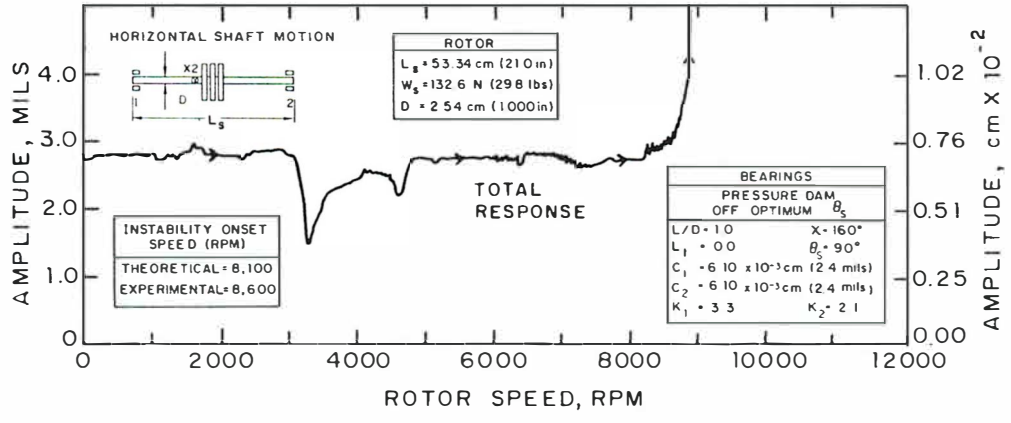

Figure 19. Total response, off-optimum step location, pressure dam bearings.

Table 1
Summary of Experimental-Theoretical Comparison of Pressure Dam Bearing Stability Performance

Bearing Type	K	C (mils)	θ_s (deg)	Instability Threshold Speed	
				Experimental (rpm)	Theoretical (rpm)
Two-axial-groove	–	1.8, 2.0	–	6,600	6,000
Near-optimum pressure dam	2.1, 2.4	2.2, 2.5	145	>13,800	11,100
Off-optimum K pressure dam	6.6, 8.6	2.4, 2.5	150	8,900	8,850
Off-optimum K pressure dam	11.7, 8.3	2.1, 2.4	140	7,800	7,800
Off-optimum θ_s pressure dam	3.3, 2.1	2.4, 2.4	90	8,600	8,100

The results of this study are summarized in Table 1. The theoretical stability analysis predicts the general trends in the experimental data. All step bearing designs increase the instability onset speed over the two-axial-groove case. Comparing all step bearing cases, the near-optimum designs have the highest onset speeds and the off-optimum designs the lowest. These results clearly illustrate the trends discussed in the previous section. As the clearance ratio increases from the near-optimum case, the instability threshold speed decreases. Also, as the location of the step decreases from the near-optimum to $\theta_s = 90°$, a drop in onset speed is evident.

DESIGN OPTIMIZATION

Incorporating all of the data presented in the previous sections, design guidelines can be deduced to optimize the stability performance of pressure dam bearings. These suggested design rules are summarized below:

1. Clearance ratios should range from the optimum of K = 3.0 to K = 6.0. Values under 3.0 should be avoided due to the sudden loss in load capacity for K < 2.0.
2. Steps should be located at about 75% of the total arclength of the pad. For the pressure dam bearing of Figure 6 with two 20° oil feed grooves, 75% of the arclength results in a step located at $\theta_s = 125°$. Larger θ_s values are preferable especially in the higher Sommerfeld number range ($S \geq 2.0$). A reasonable compromise value is $\theta_s = 140°$. Steps should not be located at θ_s values below 125°.
3. The optimum Sommerfeld number range for designing a pressure dam bearing to increase stability is $S \geq 2.0$. In the moderate Sommerfeld number range ($0.2 \leq S \leq 2.0$), the instability onset speed may be increased over a plain bearing by a factor of around 1.5.
4. Designing a bearing with a grooved lower half should be avoided due to the high operating eccentricity ratio. Load problems may develop at idle or slow rolling speeds. Exceptions are for gear box bearings where the gear load decreases with decreasing speed.
5. Since turbulent flow adds energy and consequently load, pockets should be designed to promote turbulence. This may be accomplished by specifying a surface roughness of 125 to 250 micro-inches inside the pocket. This surface roughness often results from the milling process and no additional machining steps are necessary, thereby reducing manufacturing costs. The rough surface should assist in establishing a turbulent flow regime in the pocket area.

6. Since inertia effects decrease the load capacity of the stepped pocket, reducing these effects may be beneficial even though they are of the order of 10% for oil bearings. To accomplish this, the step should not be made sharp. It should remain the radius of the cutting blade used in milling the pocket. Without the sharp step, the effects of fluid inertia may be reduced. Again, this reduces machining costs by eliminating the hand working necessary to sharpen the step.
7. Although not discussed previously, pocket axial lengths should be 65% to 70% of the total axial bearing length.

APPLICATION

A high vibration level in excess of 3.0 mils caused numerous shutdowns of two gas expanders operating under full load. The rotors were supported on plain axial-groove bearings. Each expander drove a separate multistage centrifugal compressor through a gear-type flexible coupling. The two expander-compressor trains are typical of the type of units utilized in the hydrocarbon separation process.

Figure 20 shows a sample frequency spectrum at 5,120 rpm and the large 34 Hz subsynchronous component just prior to trip-out. The 34 Hz vibration grew to around 2.5 mils, and the expander shut down soon after this signature was recorded.

A detailed stability analysis using actual bearing clearances indicated that the rotor-bearing system was unstable as a result of the bearings causing the reexcitation of the expander's first fundamental natural frequency. Utilizing the stepped pocket design guidelines discussed in the previous section, an optimized step bearing was designed to eliminate the oil-whirl-induced instability. A bearing stability plot is shown in Figure 21 showing the original bearing and the optimized pocket design. Note the large increase in instability onset speed for the optimized design compared to the plain axial-groove bearing.

The axial-groove bearings were removed and modified to the optimized pocket design similar to the design analyzed in Figure 21. The resulting frequency spectrum is shown in Figure 22. The 34 Hz component has been suppressed to an acceptable level that is representative of stable units in service. Both units have operated free of high vibration trip-outs since the bearing redesign was incorporated.

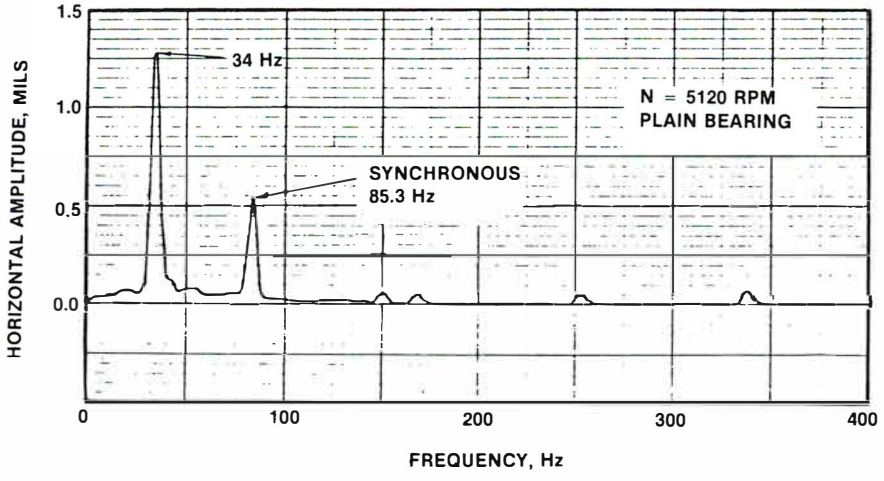

Figure 20. Frequency spectrum showing large 34 Hz component with original axial groove bearings.

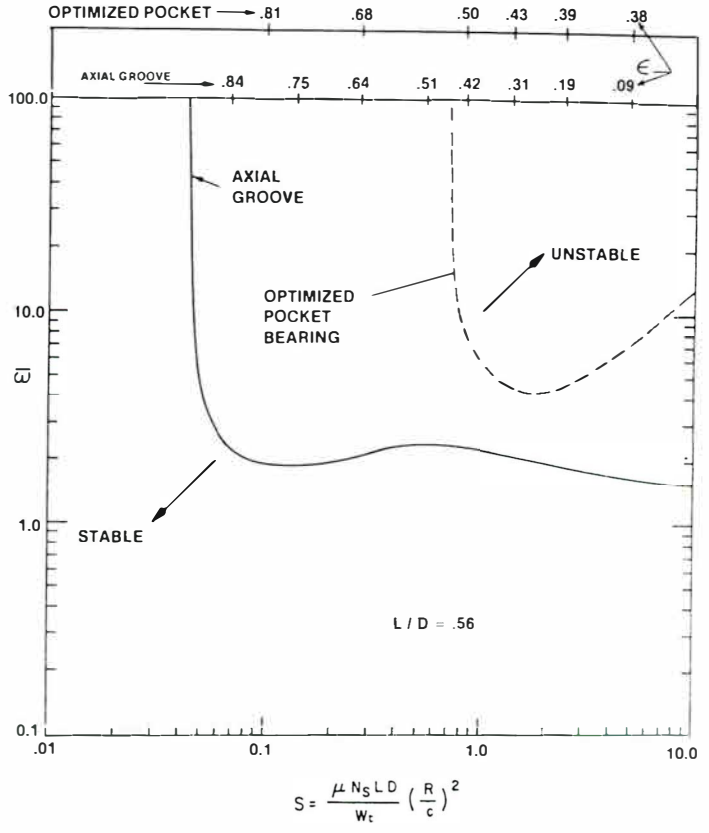

Figure 21. Optimized pocket bearing compared to the axial groove bearing, stability and load capacity.

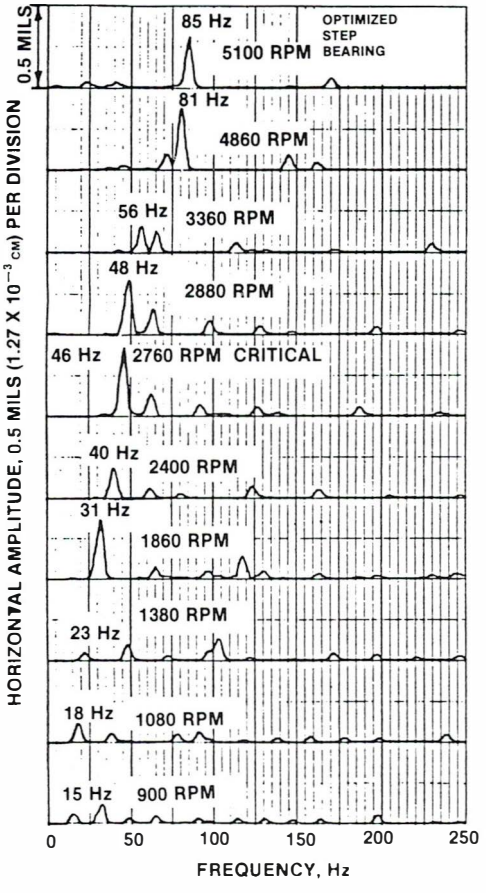

Figure 22. Frequency spectrum showing suppressed 34 Hz component with optimized step bearings.

CONCLUSION

While the pressure dam or step journal bearings will not solve all rotordynamic instability problems, it remains an extremely effective, low cost anti-whirl bearing. If near optimum clearance ratios and step locations are used, many oil whirl instabilities may be eliminated with pocket bearing designs. The design guidelines summarized in this paper should prove extremely useful in designing or retrofitting step bearings in industrial applications.

NOTATION

c bearing radial clearance, in.
c_d pocket radial clearance, in.
D shaft or journal diameter, in.
e bearing eccentricity, in.
K c_d/c = clearance ratio, dim
L bearing axial length, in.
L_s bearing span, in.
ℓ $\ell_1 + \ell_2$ = total slider length, in.
ℓ_1 pocket circumferential length (pocket length, slider bearing), in.
ℓ_2 circumferential length minus pocket (bearing length minus pocket, slider bearing), in.
L_d, L_t pocket axial length, relief track axial length, in.
$\bar{L}_d$, $\bar{L}_t$ pocket axial length ratio, relief track axial length ratio, dim
N, N_s shaft rotational speed, rpm, rps
N_t bearing instability threshold speed, rpm
O_b, O_j bearing, journal center
P hydrodynamic pressure, slider bearing, lb/in.^{2}
$\bar{P}$ $\dfrac{P}{\frac{1}{2}\rho V^2}$ = nondimensional hydrodynamic pressure, slider bearing
R shaft or journal radius, in.
R_e $\dfrac{\pi R N \rho c}{30\mu}$ = bearing Reynolds number, dim
S $\dfrac{\mu N_s L D}{W_t}\left(\dfrac{R}{c}\right)^2$ = Sommerfeld number
V slider, velocity, in./s
W_t bearing external load, lb
W hydrodynamic load generated by pocket, slider bearing, lb/in.
$\bar{W}$ $\dfrac{W}{\frac{1}{2}\rho V^2 c}$ = nondimensional pocket load, slider bearing
W_s rotor weight, lb
X, Y coordinate system for rotating journal in bearing
x horizontal coordinate, slider bearing, in.

Greek Symbols

ϵ e/c = bearing eccentricity ratio, dim
θ_s location of step measured with rotation from positive horizontal ($+X$) axis, deg
μ average lubricant viscosity, lb-s/in.^{2}
χ pad arclength exclusive of oil feed grooves, deg
ρ average lubricant density, lb-s^2/in.^{4}
$\bar{\omega}$ bearing stability parameter, dim
ω_j journal rotational speed, s^{-1}

REFERENCES

1. Nicholas, J. C., Gunter, E. J., and Barrett, L. E., "The Influence of Tilting Pad Bearing Characteristics on the Stability of High Speed Rotor-Bearing Systems," *Topics in Fluid Film Bearing and Rotor Bearing System Design and Optimization*, an ASME publication, April 1978.
2. Poritsky, H., "Contribution to the Theory of Oil Whip," *Journal of Applied Mechanics, Trans. ASME* (August 1953) pp. 1153–1161.
3. Hori, Y., "A Theory of Oil Whip," *Journal of Applied Mechanics, Trans. ASME* (June 1959) pp. 189–198.
4. Wilcock, D. F., and Booser, E. R., "Bearing Design and Application," McGraw-Hill, New York, 1957.

5. Allaire, P. E., Nicholas, J. C., and Barrett, L. E., "Analysis of Step Journal Bearings-Infinite Length, Inertia Effects," *ASLE Trans.*, Vol. 22, No. 4 (October 1979) pp. 333–341.
6. Nicholas, J. C., and Allaire, P. E., "Analysis of Step Journal Bearings-Finite Length, Stability," *ASLE Trans.*, Vol. 23, No. 2 (April 1980) pp.197–207.
7. Nicholas, J. C., Allaiire, P. E., and Lewis, D. W., "Stiffness and Damping Coefficients for Finite Length Step Journal Bearings," *ASIE Trans.*, Vol. 23, No. 4 (October 1980) pp. 353–362.
8. Nicholas, J. C., Barrett, L. E., Leader, M. E., "Experimental-Theoretical Comparison of Instability Onset Speeds for a Three Mass Rotor Supported by Step Journal Bearings," *Journal of Mechanical Design, Trans. ASME*, Vol. 102, No. 2 (April 1980) pp. 344–351.
9. Nicholas, J. C., Kirk, R. G., "Selection and Design of Tilting Pad and Fixed Lobe Journal Bearings for Optimum Turborotor Dynamics," *Proceedings of the Eight Turbomachinery Symposium*, Texas A & M University, College Station, Texas, November 1979.
10. Flack, R. D., Leader, M. E., and Allaire, P. E., "Experimental and Theoretical Pressures in Step Journal Bearings," *ASLE Trans.*, Vol. 24, No. 3 (July 1981) pp. 316–322.
11. Allaire, P. E., "Design of Journal Bearings for High Speed Rotating Machinery," *Fundamentals of the Design of Fluid Film Bearings*, an ASME publication. (1979) pp. 45–84.
12. Lund, J. W., and Thomsen, K. K., "A Calculation Method and Data for the Dynamic Coefficients of Oil-Lubricated Journal Bearings," *Topics in Fluid Film Bearing and Rotor Bearing System Design and Optimization*, an ASME publication (April 1978) pp. 1–28.
13. Kirk, R. G., "The Influence of Manufacturing Tolerances on Multi-Lobe Bearing Performance in Turbomachinery," *Topics in Fluid Film Bearing and Rotor Bearing System Design and Optimization*, an ASME publication (April 1978) pp. 108–129.
14. Akkok, M., and Ettles, C. M., "The Effect of Grooving and Bore Shape on the Stability of Journal Bearings," *ASLE Trans.*, Vol. 23, No. 4 (October 1980) pp. 431–441.
15. Allaire, P. E., Nicholas, J. C., and Gunter, E. J., "Systems of Finite Elements for Finite Bearings," *Journal of Lubrication Technology, Trans. ASME*, Vol. 98, No. 2 (April 1977) pp. 187–197.
16. Constantinescu, V. N., and Galetuse, S., "Pressure Drop Due to Inertia Forces in Step Bearings," *Journal of Lubrication Technology, Trans. ASME*, Vol. 98, No. 1 (January 1976) pp. 167–174.
17. Leader, M. E., Flack, R. D., and Allaire, P. E., "Experimental Study of Three Journal Bearings with a Flexible Rotor," *ASLE Trans.*, Vol. 23, No. 4 (October 1980) pp. 363–369.
18. Flack, R. D., Leader, M. E., and Gunter, E. J., "An Experimental Investigation on the Response of a Flexible Rotor Mounted in Pressure Dam Bearings," *Journal of Mechanical Design, Trans. ASME*, Vol. 102, No. 4 (October 1980) pp. 842–850.

RMT

Rotating Machinery Technology, Inc.
4181 Bolivar Road
Wellsville, NY 14895
716-593-3700
716-593-2693 (fax)